Technology and Health Care 28 (2020) S13–S24
DOI 10.3233/THC-209003
IOS Press

Modeling and simulation of excitation-contraction coupling of fast-twitch skeletal muscle fibers

Monan Wang*, Jiangang Sun and Qiyou Yang
Key Laboratory of Medical Biomechanics and Materials of Heilongjiang Province, Harbin University of Science and Technology, Harbin, Heilongjiang, 150080, China

Abstract.
BACKGROUND: The current excitation-contraction coupling model of fast-twitch skeletal muscle fibers cannot completely simulate the excitation-contraction process.
OBJECTIVE: To solve this problem, this study proposes an excitation-contraction model of fast-twitch skeletal muscle fibers based on the physiological structure and contractile properties of half-sarcomeres.
METHODS: The model includes the action potential model of fast-twitch fiber membranes and transverse tubule membranes, the cycle model of Ca^{2+} in myofibril, the cross-bridge cycle model, and the fatigue model of metabolism.
RESULTS: Finally, detailed analyses of the results from the simulation are conducted using the Simulink toolbox in MATLAB. Two conditions, non-coincidence and coincidence, are analyzed for both the thick and thin myofilaments.
CONCLUSIONS: The simulation results of two groups of models are the same as the previous research results, which validates the accuracy of models.

Keywords: Skeletal muscles, fast-twitch fiber, excitation-contraction coupling, simulation

1. Introduction

At present, the action potential of the sarcolemma and transverse tubule membranes are studied using the Hodgkin-Huxley model and the Goldman-Hodgkin-Katz equation. The inwardly rectifying potassium (Kir) channel, together with the chloride channel (ClC-1), plays a vital role in the skeletal muscle physiology. Current research primarily focuses on the fibrous surface and transverse tubular system (TTS) of amphibians [1], and the measurement of Kir of mammalian skeletal muscle fibers [2–4]. The primary physiological function of mammalian skeletal muscle is to maintain the stability of resting membrane potential and to enable the excitation of electrogenic cells. It is essential to study the properties of Kir in mammalian skeletal muscle fibers to further understand the related muscular diseasesin humans [5–7].

In vertebrate skeletal muscle fibers, action potential controls contractile activity by inducing rapid changes of the free Ca^{2+} concentration in the sarcoplasm. Ca^{2+}, thus, plays a role in triggering and

*Corresponding author: Monan Wang, Key Laboratory of Medical Biomechanics and Materials of Heilongjiang Province, Harbin University of Science and Technology, Xuefu Road, Harbin, Heilongjiang, 150080, China. Tel.: +86 451 86390530; Fax: +86 451 86390500; E-mail: qqwmnan@163.com.

0928-7329/20/$35.00 © 2020 – IOS Press and the authors. All rights reserved
This article is published online with Open Access and distributed under the terms of the Creative Commons Attribution Non-Commercial License (CC BY-NC 4.0).

regulating skeletal muscle contraction, and its concentration affects contractile force and speed. In order to regulate Ca^{2+} in a myofibril accurately, according to the physiological structure properties of the sarcomere, researchers have used half-sarcomeres and divide its space [8] to analyze the change of Ca^{2+} concentration in the corresponding regions [9–11]. The Ca^{2+} indicator, with low affinity, is microinjected into the sarcoplasm to evaluate the amplitude and time historyof regional spatial variation of mean Ca^{2+} concentration [12]. This model can be used to evaluate the movement of Ca^{2+} in myofibrils, the release of Ca^{2+} in sarcoplasmic reticulum, the combination of Ca^{2+} in sarcoplasm, and primary buffers (such as troponin, ATP, parvalbumin, and sarcoplasmic reticulum Ca^{2+} pump). The Ca^{2+} in sarcoplasm is recycled to the sarcoplasmic reticulum by the Ca^{2+} pump.

Skeletal muscle fibers exhibit contractility through the relative sliding of the sarcomere's thick and thin myofilaments in the myofibril. The sliding process depends on the hydrolysis coupling of ATP and the circulation of the fine filaments, i.e., actin filaments, along the molecules on the head of myosin, forming cross-bridges. In striated muscle fibers, it is believed that tropomyosin and troponin prevent the binding of myosin and actin, which form the cross-bridge circulation and act as doormen. Tropomyosin is the basis of many of actin's biological activities, and the movement of troponin on the surface of actin is considered critical to the cooperative allosteric regulation of actin. The different positions of the thick and thin myofilaments will affect the speed at which Ca^{2+} and troponin combine and separate [13]. Skeletal muscle fibers become fatigued during the excitation-contraction process, and many factors affect fatigue. Metabolic fatigue is a multi-factored regulation process that includes the accumulation of phosphate, cross-bridge circulation, and reduction of calcium in the sarcoplasmic reticulum [14].

The currently existing excitation-contraction model of fast-twitch muscle fibers cannot simulate the excitation-contraction process completely. To solve this problem, this study proposes an excitation-contraction model for fast-twitch skeletal muscle fibers based on the physiological structure and contractile properties of the half-sarcomere. The study is structured as follows: (1) establishment of an action potential model for fast-twitch muscle fiber membranes and transverse tubule membranes; (2) establishment of the cycle model of Ca^{2+} in myofibril; (3) establishment of the cross-bridge cycle model and the fatigue model of metabolism in half-sarcomeres; and (4) analysis of the results from the excitation-contraction model simulation.

2. Methods

2.1. Modeling of the skeletal fast muscle fiber membrane potential

A two-compartment model was used to simulate the action potential of skeletal fast muscle fibers. The total ionic current on the surface of the muscle fibers is calculated by adding Na^+ current ($I_{Na,s}$), K^+ delayed rectifier current ($I_{DR,s}$), K^+ inward rectifier current ($I_{IR,s}$), Cl^- current ($I_{Cl,s}$), and $Na^+ - K^+$ current ($I_{NaK,s}$), as shown by Eq. (1):

$$I_{ionic,s} = I_{Na,s} + I_{DR,s} + I_{IR,s} + I_{Cl,s} + I_{NaK,s} \tag{1}$$

Due to the difference between ion channel densities in the T tube and myolemma, the ratio of T tube membrane channel density to myolemma channel density can be represented by η. The calculation of ionic current ($I_{ionic,t}$) on the T tube per unit area is then shown by Eq. (2) as:

$$\begin{aligned} I_{ionic,t} = {} & \eta_{Na} g_{Na,t}(J_{Na,t}/75) + \eta_{DR} g_{DR,t}(J_{k,t}/50) + \eta_{IR} g_{IR,t}(J_{K,t}/50) \\ & + \eta_{Cl} g_{Cl,t}(J_{Cl,t}/75) + \eta_{NaK}\overline{I_{NaK,t}} f_t, \end{aligned} \tag{2}$$

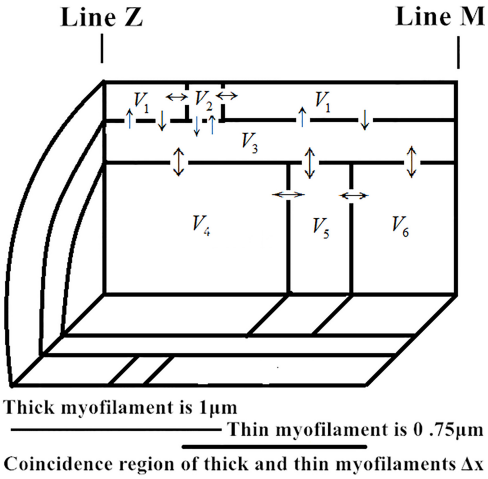

Fig. 1. Geometric division diagram of half sarcomere.

where $g_{Na,t}$ is the Na^+ channel conductance, $g_{DR,t}$ is the K^+ channel conductance, $g_{IR,t}$ is the K^+ inward rectifier channel conductance, and $g_{Cl,t}$ is the Cl^- channel conductance.

The changes inconcentration of $Na^+(Na_i)$ in cells, $Na^+(Na_t)$ in T tube, and $Na^+(Na_e)$ in intercellular space are shown in Eqs (3)–(5), using time as the basis. Similarly, the changes inconcentration (with respect to time) of $K^+(K_i)$ in cells, $K^+(K_t)$ in T tube, and $K^+(K_e)$ in intercellular space can be obtained.

$$\frac{dNa_i}{dt} = \frac{-f_T(I_{Na,t} + 3I_{NaK,t} + I_{Na}^{rest})}{1000F\xi_1} - \frac{I_{Na,s} + 3I_{NaK,s} + I_{Na}^{rest}}{1000F\xi_2} \tag{3}$$

$$\frac{dNa_t}{dt} = \frac{I_{Na,t} + 3I_{NaK,t} + I_{Na}^{rest}}{1000F\xi_1} - \frac{Na_t - Na_e}{\tau_{Na_1}} \tag{4}$$

$$\frac{dNa_e}{dt} = \frac{I_{Na} + 3I_{NaK} + I_{Na}^{rest}}{1000F\xi_3} - \frac{Na_t - Na_e}{\tau_{Na_2}} \tag{5}$$

In Eqs (2)–(5), f_T represents the proportion of fiber occupied by the T tube, ξ_1 represents the ratio of volume to surface area of the T tube, ξ_2 represents the ratio of volume to surface area of cells, ξ_3 represents the ratio of volume to surface area of intercellular space, τ_{Na_1} represents diffusion time constant of the T tube, and τ_{Na_2} represents the diffusion time constant of intercellular space.

2.2. Modeling of calcium cyclingin skeletal fast muscle fiber

We divided the sarcomere into six geometric regions, which are V_1, V_2, V_3, V_4, V_5, and V_6, as shown in Fig. 1. $V_1 = 5.5\%V$, $V_2 = 3.5\%V$, $V_3 = 6\%V$, $V_4 = 85\%\left(1 - \frac{0.75}{l_x}\right)V$, $V_5 = 85\%\left(\frac{1.75}{l_x} - 1\right)V$, and $V_6 = 85\%\left(1 - \frac{1}{l_x}\right)V$.

A 10-state model is used to describe the release process from the T tube voltage to the Reynolds channel. The ten states consist of five states of four voltage sensor molecules and two states of a Reynolds channel (including five closed states ($C_0 - C_4$) and five open states). Based on the division of the half-sarcomere regions and the Ca^{2+} cycle, the change in Ca^{2+} concentration in $V_1 - V_6$ regions are analyzed, as shown in Eqs (6)–(11), and the model's parameters are shown in Table 1:

Table 1
Model parameters

Parameter	Unit	Value	Parameter	Unit	Value
Par_{tot}	μM	1500	$k^{off}_{Ca,Par}$	ms^{-1}	0.0005
Cs_{tot}	μM	31000	$k^{on}_{Ca,ATP}$	$\mu M^{-1}ms^{-1}$	0.15
K_{SR}	μM	1	$k^{off}_{Ca,ATP}$	ms^{-1}	30
υ_{SR}	$\mu M ms^{-1}\mu m^{-3}$	4.875	$k^{on}_{Mg,Par}$	$\mu M^{-1}ms^{-1}$	3.3×10^{-5}
L_e	$\mu m^3 ms^{-1}$	2×10^{-5}	$k^{off}_{Mg,Par}$	ms^{-1}	0.003
$\tau_R = \tau^{SR}_R$	$\mu m^3 ms^{-1}$	0.75	$k^{on}_{Mg,ATP}$	$\mu M^{-1}ms^{-1}$	1.5×10^{-3}
τ_{ATP}	$\mu m^3 ms^{-1}$	0.375	$k^{off}_{Mg,ATP}$	ms^{-1}	0.15
τ_{Mg}	$\mu m^3 ms^{-1}$	1.5	$k^{on}_{Ca,Cs}$	$\mu M^{-1}ms^{-1}$	4×10^{-6}
$k^{on}_{Ca,Par}$	$\mu M^{-1}ms^{-1}$	0.0417	$k^{off}_{Ca,Cs}$	ms^{-1}	0.005
i	$\mu m^3 ms^{-1}$	300			

$$\frac{dCa_1}{dt} = \frac{\upsilon_{SR}Ca_3}{(Ca_3 + K_{SR})V_1} - \frac{L_e(Ca_1 - Ca_3)}{V_1} - \frac{\tau^{SR}_R(Ca_1 - Ca_2)}{V_1} \tag{6}$$

$$\begin{aligned}\frac{dCa_2}{dt} = {} & \frac{-i(O_0 + O_1 + O_2 + O_3 + O_4)(Ca_2 - Ca_3)}{V_2} + \frac{\upsilon_{SR}Ca_3}{(Ca_3 + K_{SR})V_2} \\ & - \frac{L_e(Ca_2 - Ca_3)}{V_2} + \frac{\tau^{SR}_R(Ca_1 - Ca_2)}{V_2} + (k^{off}_{Ca,Cs}Ca_2^{Cs} - k^{on}_{Ca,Cs}Ca_2(Cs_{tot} - Ca_2^{Cs}))\end{aligned} \tag{7}$$

$$\begin{aligned}\frac{dCa_3}{dt} = {} & \frac{i(O_0 + O_1 + O_2 + O_3 + O_4)(Ca_2 - Ca_3)}{V_3} - \frac{2\upsilon_{SR}Ca_3}{(Ca_3 + K_{SR})V_3} \\ & + \frac{L_e(Ca_1 - Ca_3)}{V_3} + \frac{L_e(Ca_2 - Ca_3)}{V_3} - \frac{\tau_R(3Ca_3 - Ca_4 - Ca_5 - Ca_6)}{V_3} \\ & - (k^{on}_{Ca,Par}Ca_3(Par_{tot} - Ca_3^{Par} - Mg_3^{Par}) - k^{off}_{Ca,Par}Ca_3^{Par}) \\ & - (k^{on}_{Ca,ATP}Ca_3ATP_3 - k^{off}_{Ca,ATP}Ca_3^{ATP})\end{aligned} \tag{8}$$

$$\begin{aligned}\frac{dCa_4}{dt} = {} & \frac{\tau_R(Ca_3 - 2Ca_4 + Ca_5)}{V_4} - (k^{on}_{Ca,Par}Ca_4(Par_{tot} - Ca_4^{Par} - Mg_4^{Par}) - k^{off}_{Ca,Par}Ca_4^{Par}) \\ & - (k^{on}_{Ca,ATP}Ca_4ATP_4 - k^{off}_{Ca,ATP}Ca_4^{ATP}) - F_1(Ca_4, T_n)\end{aligned} \tag{9}$$

$$\begin{aligned}\frac{dCa_5}{dt} = {} & \frac{\tau_R(Ca_3 + Ca_4 - 3Ca_5 + Ca_6)}{V_5} - (k^{on}_{Ca,Par}Ca_5(Par_{tot} - Ca_5^{Par} - Mg_5^{Par}) - k^{off}_{Ca,Par}Ca_5^{Par}) \\ & - (k^{on}_{Ca,ATP}Ca_5ATP_5 - k^{off}_{Ca,ATP}Ca_5^{ATP}) - F_2(Ca_5, T_n)\end{aligned} \tag{10}$$

$$\begin{aligned}\frac{dCa_6}{dt} = {} & \frac{\tau_R(Ca_3 + Ca_5 - 2Ca_6)}{V_6} - (k^{on}_{Ca,Par}Ca_6(Par_{tot} - Ca_6^{Par} - Mg_6^{Par}) - k^{off}_{Ca,Par}Ca_6^{Par}) \\ & - (k^{on}_{Ca,ATP}Ca_6ATP_6 - k^{off}_{Ca,ATP}Ca_6^{ATP})\end{aligned} \tag{11}$$

2.3. Modeling of the cross-bridge dynamic in skeletal fast muscle fiber

A 6-state model is used when Ca^{2+} and troponin combine in the non-coincidence region (V_4), and the binding site of free troponin (T_0) is shown in Eq. (12):

$$T_0 = T_{tot} - Ca_4^T - Ca_4^{Ca_4^T} - D_0 - D_1 - D_2 \tag{12}$$

Table 2
Model parameters

Parameter	Unit	Value	Parameter	Unit	Value
T_{tot}	μM	140	k_2^{on}	ms^{-1}	0.15
$k_{Ca,T}^{on}$	$\mu M^{-1}ms^{-1}$	0.04425	k_2^{off}	ms^{-1}	0.05
$k_{Ca,T}^{off}$	ms^{-1}	0.115	f_p	ms^{-1}	15
k_0^{on}	ms^{-1}	0	f_0	ms^{-1}	1.5
k_0^{off}	ms^{-1}	0.15	h_p	ms^{-1}	0.18
k_1^{on}	ms^{-1}	0	h_0	ms^{-1}	0.24
k_1^{off}	ms^{-1}	0.12	g_0	ms^{-1}	0.12

In the non-coincidence region (V_4) the function of combining Ca^{2+} and troponin, $F_1(Ca_4, T_n)$, is calculated according to Eq. (13):

$$\begin{aligned} F_1(Ca_4, T_n) = {} & k_T^{on} Ca_4 T_0 - k_T^{off} Ca_4^T + k_T^{on} Ca_4 Ca_4^T - k_T^{off} Ca_4^{Ca_4^T} + k_T^{on} Ca_4 D_0 - k_T^{off} D_1 \\ & + k_T^{on} Ca_4 D_1 - k_T^{off} D_2 \end{aligned} \tag{13}$$

In the coincidence region (V_5), an 8-state model is used. During the process of cross-bridge cycling, the binding site of free troponin (T_0) is shown in Eq. (14):

$$T_0 = T_{tot} - Ca_5^T - Ca_5^{Ca_5^T} - D_0 - D_1 - D_2 - A_1 - A_2 \tag{14}$$

In the coincidence region (V_5), during the process of cross-bridge cycling, the function of combining Ca^{2+} and troponin, $F_2(Ca_5, T_n)$, is calculated according to Eq. (15), and the model's parameters are shown in Table 2.

$$\begin{aligned} F_2(Ca_5, T_n) = {} & k_T^{on} Ca_5 T_0 - k_T^{off} Ca_5^T + k_T^{on} Ca_5 Ca_5^T - k_T^{off} Ca_5^{Ca_5^T} + k_T^{on} Ca_5 D_0 - k_T^{off} D_1 \\ & + k_T^{on} Ca_5 D_1 - k_T^{off} D_2 \end{aligned} \tag{15}$$

2.4. The fatigue modeling of metabolismin skeletal fast muscle fiber

During the cross-bridge cycle, when the cross-bridge attains a strong binding state from a weak binding state, the ATP will be hydrolyzedto generate ADP and P_i. When the product of solubilities of P_{iSR} and Ca_1 in sarcoplasmic reticulum exceeds 6 mM^2, it is considered that the P_i in sarcoplasmgoes through the passive channel and is transported to the sarcoplasmic reticulum,at a speed ranging from 30 to 170 μm/s, and combines with Ca^{2+} in the sarcoplasmic reticulum to generate precipitation. A P_i of 20 mM can reduce 29% of Ca^{2+} released by sarcoplasmic reticulum. When the muscle fiber contraction ends, P_i in sarcoplasm can slowly be removed, and the sarcoplasm would then recover to a resting state of 3 mM.

3. Results and discussion

3.1. Analysis of the simulated excitation-contraction model of skeletal fast muscle fiber in conditions of non-coincidence of the thick and thin myofilaments

When skeletal fast muscle fibers are in a resting state, the number of ions in the myofibrilremains constant, and their concentrations are shown in Table 3. Calsequestrin in the sarcoplasmic reticulum combines a large amount of calcium ions to be stored. Magnesium ions in sarcoplasm combine at most of

Table 3
Ion concentration in the myofibril at resting

Ions	Concentration	Unit
Calsequestrin (sarcoplasmic reticulum)	31000	μM
Ca^{2+} (sarcoplasmic reticulum)	1500	μM
Ca^{2+} (sarcoplasm)	0.05	μM
Mg^{2+} (sarcoplasm)	1000	μM
ATP (sarcoplasm)	8000	μM
Parvalbumin (sarcoplasm)	1500	μM
Troponin (sarcoplasm)	240	μM

Table 4
The percentage of ions in the binding site at resting

Conjugates / Ions	Ca^{2+}	Mg^{2+}
Calsequestrin (sarcoplasmic reticulum)	54.55%	–
Troponin (sarcoplasm)	7.1%	–
Parvalbumin (sarcoplasm)	41%	54.1%
ATP (sarcoplasm)	–	90.9%

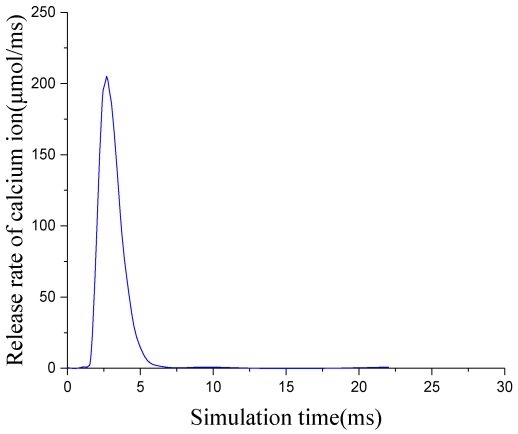

Fig. 2. Release rate of calcium ion in terminal cistern.

the ATP binding sites. The percentages of calcium and magnesium ions in binding sites, respectively, are shown in Table 4.

When a single action potential is transmitted to the transverse tubule membranes, the dihydropyridine voltage receptor (DHPR) on the transverse tubule membranes is coupled to the Reynolds channel on the terminal cistern to control the release of Ca^{2+} on the terminal cistern. According to the mathematical model established in this study, a simulation module is built in Simulink to simulate the release of Ca^{2+} on the terminal cistern membrane under the control of a single action potential. The simulation results are shown in Fig. 2. The terminal cistern began to release the Ca^{2+} 1.4 ms after the action potential was generated, the peak value of the release flow was 204 μM/ms, and the time corresponding to the peak value was 2.8 ms. The simulation results were the same asthe mean value detected by Baylor et al., upon calculation of the Ca^{2+} fluoresce in of 11 muscle fibers. When Ca^{2+} was released into the sarcoplasm, it bound to the binding sites of the buffer in the sarcoplasm, such as ATP and parvalbumin. In the V4 region, besides ATP and parvalbumin, troponin was also included. Considering the V4 region as an example,

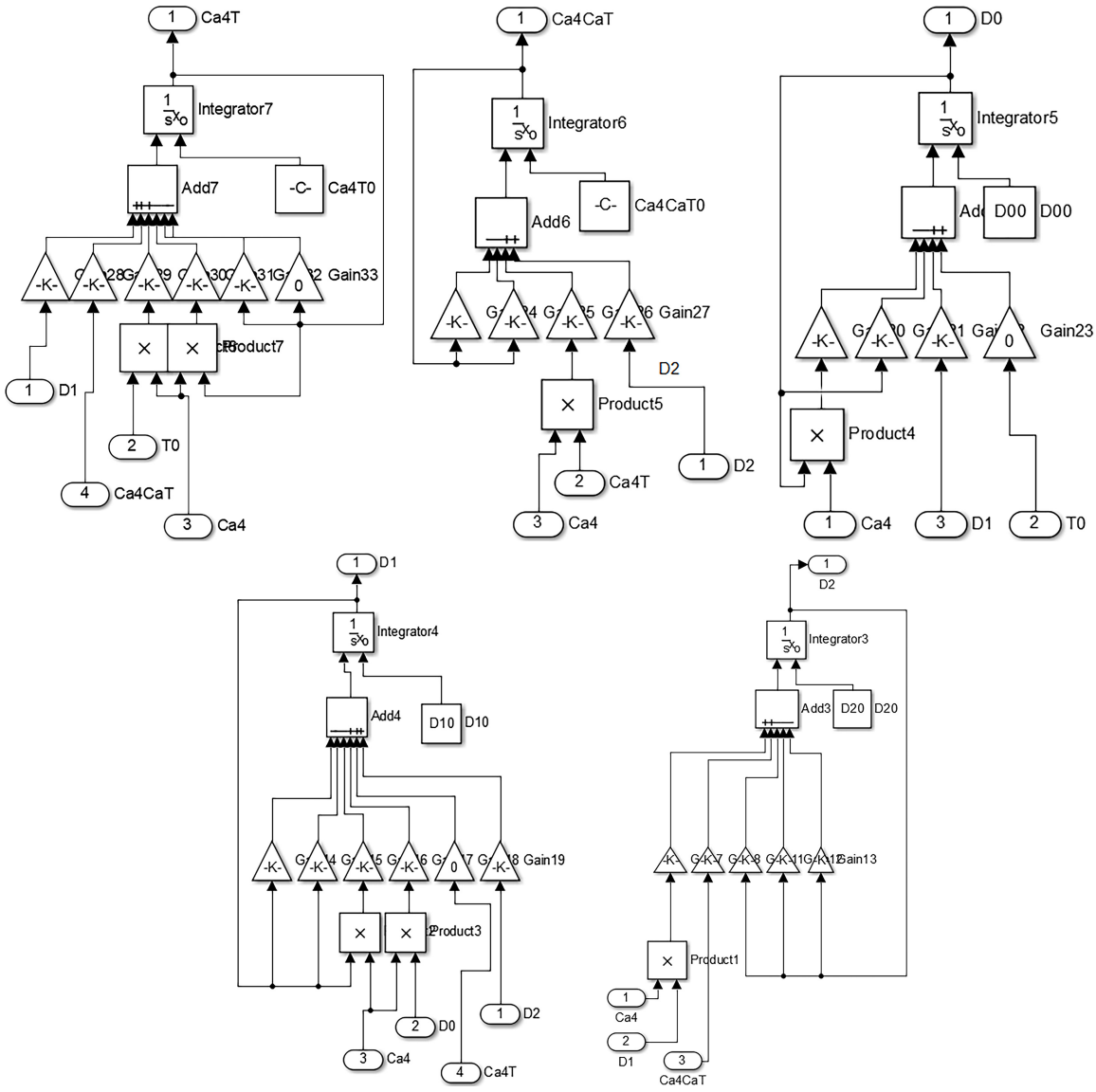

Fig. 3. The simulation module of the binding of calcium ion and troponin.

the simulation process carried out in Simulink can be described as follows: (1) in the V4 region, the calcium ion and troponin are bound with a 6-state model; (2) a blank model editing window is opened in Simulink; (3) the corresponding modules are created; (4) the parameters of the module are set and the values are shown in Table 4; and (5) the modules are connected, as shown in Fig. 3. The simulation processes for the other regions are similar to those employed for the V4 region. The modules built in Simulink are connected to form the excitation-contraction model of fast-twitch skeletal muscle fibers when non-coincidence of the thick and thin myofilaments occur. The module system is shown in Fig. 4. The system parameters of the model are set, the start time of the simulation is set to 0, the stop time of the simulation is set to 30, and the type is set to Variable-step [15].

The simulation results showed that the concentrations of calcium ions in V3, V4, and V5 regions

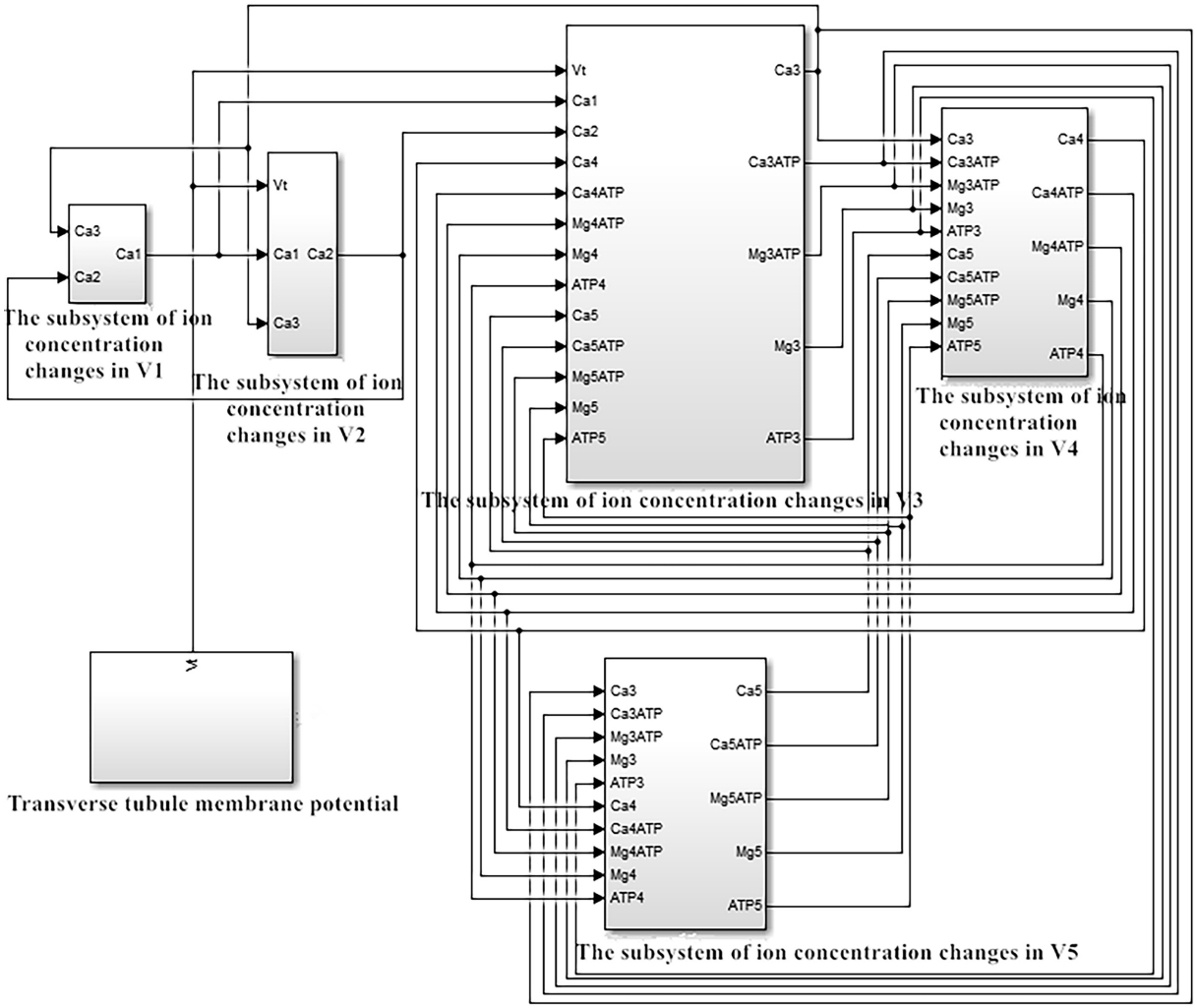

Fig. 4. The simulation system of the excitation-contraction model of fast-twitch fiber of skeletal muscle when non-coincidence of the thick and thin myofilaments occurs.

increased after 1.4 ms, and the concentrations of free calcium ions in V3 reached a peak value of 24 μM at 3.5 ms. With the diffusion of free calcium ions, the concentrations of calcium ions in V4 and V5 also reached peak values. When the action potential was stopped, the calcium pump began to transport the calcium ions from the sarcoplasm to the sarcoplasmic reticulum, which led to the decrease of the calcium ion concentration in the sarcoplasm, upon which it attained resting state. As shown in Fig. 5, Baylor and Hollingworth measured the change of calcium ion concentration by injecting the calcium ion indicator, furaptra, into the fast-twitch muscle fibers of mice. The peak value of free calcium ion concentration measured was 17 μM, and the time corresponding to the peak value was 4.2 ms. Baylor's simulation by a multi-compartment model showed that the average free calcium ion concentration in sarcoplasm was 16.3 μM, and the corresponding time was 3.5 ms. The simulation results in this study show that the average free calcium ion concentration in sarcoplasm is 16 μM, and the time corresponding to the peak value is 3.2 ms. The free Ca^{2+} concentration amplitude in this study are similar to the experimental results and Baylor's simulation results, and the time taken for free calcium ion concentration to reach the

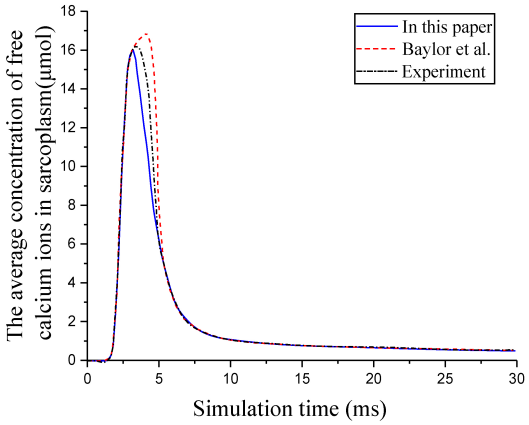

Fig. 5. The average concentration of free calcium ions in sarcoplasm.

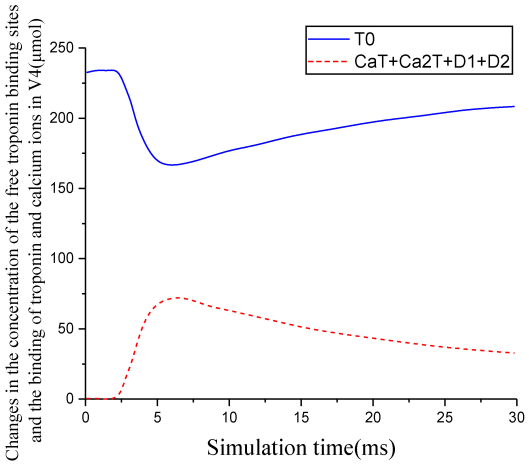

Fig. 6. Changes in the concentration of the free troponin binding sites and the binding of troponin and calcium ions in V4.

peak value is slightly smaller than that in Baylor's study. The small size of the half-sarcomere used in this model may have led to the free calcium ion concentration in the sarcoplasm reaching the peak value more quickly. In the region of V4, Ca^{2+} binds to troponin. Since the thick and thin myofilaments do not overlap, there is no cross-bridge activation, and the 6-state model is used to combine Ca^{2+} and troponin. The simulation results of the binding of Ca^{2+} and troponin in region V4 are shown in Fig. 6. With the combination of Ca^{2+} and troponin, the concentration of tropomyosin-binding site of free troponin decreased, and its lowest value was approximately 170 μM, which was 71% of the concentration of free binding site of troponin in the resting state. The concentration of combining Ca^{2+} and troponin increased, and its maximum value was found to be 70 μM, which was 29% of the combination of calcium ions and troponin at resting state, and the corresponding time was 7 ms. Zot et al. simulated the combination of Ca^{2+} and troponin, and the peak value of free troponin binding site was 75% of that in its resting state. The peak value of the combination of calcium ion and troponin was 25% of that in its resting state, and the time corresponding to the peak value was 10 ms. In comparison to the simulation results of Zot et al. [16], the peak value obtained in this study is slightly higher, and the time corresponding to the peak value is a little shorter. However, the time corresponding to the peak value in this study is closer to that of

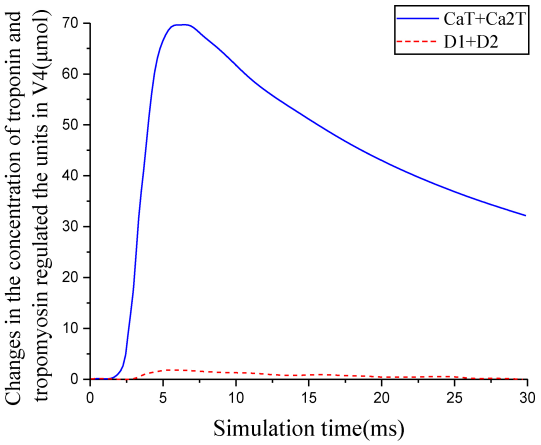

Fig. 7. Changes in the concentration of troponin and tropomyosin regulated the units in V4.

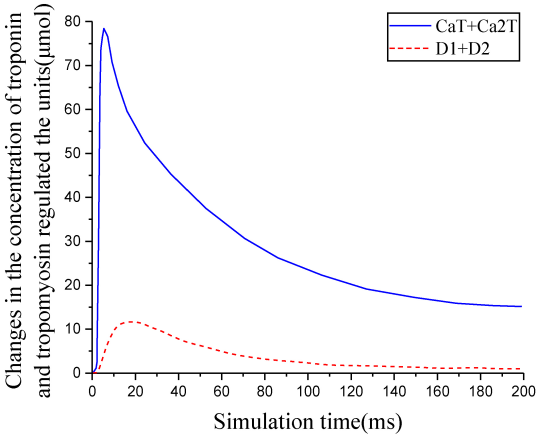

Fig. 8. Changes in the concentration of troponin and tropomyosin regulated the units.

Baylor et al. The simulation results of the relationship between troponin and tropomyosin regulated unit concentration is shown in Fig. 7. Only a small number of tropomyosin structures have conformational changes when a single action potential is stimulated.

3.2. Simulation analysis of the excitation-contraction model of skeletal fast muscle fiber in the condition of coincidence of the thick and thin myofilaments

When the half-sarcomere's length was $l_x \in [1.1, 1.75)$ μm, the thick and thin myofilaments coincided. With the shortening of the half-sarcomere, the number of the coincident thick and thin myofilaments increased; at that time, the structure of the half-sarcomere was divided into 6 regions. In region V_4, a 6-state model was used when Ca^{2+} and troponin combines. In region V_5, due to the coincidence of thick and thin myofilaments, when troponin was combined with two Ca^{2+} ions, the cross-bridge was activated, so an 8-state model was used in this region.

When $l_x = 1.1$ μm, the thick and thin myofilaments coincided completely. The conformations of troponin and tropomyosin regulated units are changed by the binding of Ca^{2+} and troponin during a single

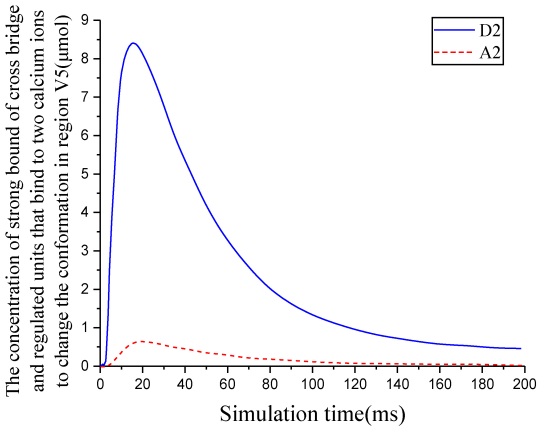

Fig. 9. Degree of cross-bridge activation.

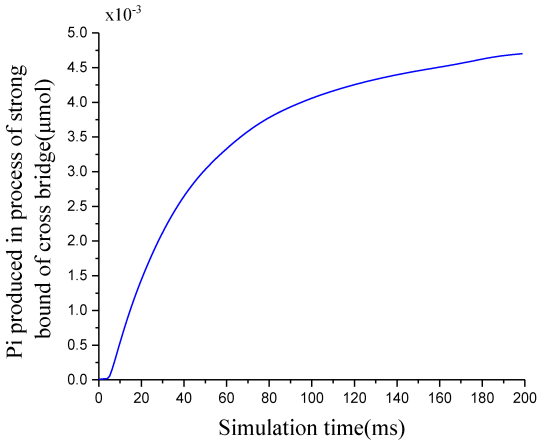

Fig. 10. ATP hydrolyzed to produce phosphate.

contraction. The head of myosin (cross bridge) on the thick myofilament binds to the myosin-binding site on the thin myofilament, actin, by hydrolyzing ATP. The simulation results of the combination of Ca^{2+} and troponin, and cross-bridge activation are shown in Fig. 8. In comparison to Fig. 7, the concentration of troponin and tropomyosin regulated units increased, and the combination of myosin to actin changed the rate of binding and separation of Ca^{2+} and troponin. This promoted the conformation change of tropomyosin and decreased the rate of separation of Ca^{2+} and troponin. The result was consistent with that of Zot's. The simulation results of the degree of cross-bridge activation are shown in Fig. 9. The degree A2 of cross-bridge activation represents the intensity of the excitation-contraction of the skeletal fast muscle fibers. The simulation results of ATP hydrolysis are shown in Fig. 10, with the circulation of the cross-bridge, and the phosphoric acid produced by hydrolysis of ATP accumulating continuously.

When the length of the half-sarcomere is $l_x \in (1.1, 1.75)$, the model can be used to simulate the change of free calcium ion concentration in the sarcoplasm, the degree of cross-bridge activation, and the P_i produced by ATP hydrolysis in the conditions of different degrees of coincidence of thick and thin myofilaments.

Acknowledgments

This research was supported by NSFC (No. 61572159, No. 61972117), the Natural Science Foundation of Heilongjiang Province of China (ZD2019E007).

Conflict of interest

None to report.

References

[1] Cannon SC, Brown RH, David JR, Corey P. Theoretical reconstruction of myotonia and paralysis caused by incomplete inactivation of sodium channels. Biophysical Journal. 1993; 65: 270-288.
[2] Stanfield PR, Nakajima S, Nakajima Y. Constitutively active and G-protein coupled inward rectifier K+ channels: Kir2.0 and Kir3.0. Rev Physiol Biochem Pharmacol. 2002; 145: 47-179.
[3] Dassau L, Conti LR, Radeke CM, Ptacek LJ, Vandenberg CA. Kir2.6 regulates the surface expression of Kir2.x inward rectifier potassium channels. J Biol Chem. 2011; 286: 9526-9541.
[4] Difranco M, Yu C, Quinonez M, Vergara JL. Inward rectifier potassium channels in mammalian skeletal muscle fibers. J Physiol. 2015; 593(5): 1213-1238.
[5] DiFranco M, Herrera A, Vergara JL. Chloride currents from the transverse tubular system in adult mammalian skeletal muscle fibers. J Gen Physiol. 2011; 137: 21-41.
[6] DiFranco M, Vergara JL. The Na conductance in the sarcolemma and the transverse tubular system membranes of mammalian skeletal muscle fibers. J Gen Physiol. 2011; 138: 393-419.
[7] DiFranco M, Quinonez M, Vergara JL. The delayed rectifier potassium conductance in the sarcolemma and the transverse tubular system membranes of mammalian skeletal muscle fibers. J Gen Physiol. 2012; 140: 109-137.
[8] Baylor SM, Hollingworth S. Model of sarcomeric Ca^{2+} movements, including ATP Ca^{2+} binding and diffusion, during activation of frog skeletal muscle. Gen. Physiol. 1998; 112: 297-316.
[9] Hollingworth S, Zeiger U, Baylor SM. Comparison of the myoplasmic calcium transient elicited by an action potential in intact fibres of mdx and normal mice. Journal of Physiology. 2008; 586: 5063-5075.
[10] Hollingworth S, Gee KR, Baylor SM. Low-affinity Ca^{2+} indicators compared in measurements of skeletal muscle Ca^{2+} transients. Biophys. J. 2009; 97: 1864-1872.
[11] Hollingworth S, Kim MM, Baylor SM. Measurement and simulation of myoplasmic calcium transients in mouse slow-twitch muscle fibres. Journal of Physiology. 2012; 590: 575-594.
[12] Baylor SM, Hollingworth S. Calcium indicators andcalcium signalling in skeletal muscle fibres during excitation-contraction coupling. Prog. Biophys. Mol. Biol. 2011; 105: 162-179.
[13] El-Mezgueldi MM. Tropomyosin dynamics. Muscle Res. Cell Motility. 2014; 35: 203-210.
[14] Lehrer SS. The 3-state model of muscle regulation revisited: Is a fourth state involved? MuscleRes. Cell Motility. 2011; 32: 203-208.
[15] Sun JG. Modeling and simulation of skeletal muscle rapid fiber excitation contraction. Harbin University of Science and Technology. 2018; 3: 25-55.
[16] Zot HG, Hasbun JE. Modeling Ca^{2+}-bound troponin in excitation contraction coupling. Frontiers in Physiology. 2016; 7(406): 1-10.